

## Structure variation in low cordierites

JAMES H. WALLACE AND HANS-RUDOLF WENK

*Department of Geology and Geophysics  
University of California, Berkeley, California 94720*

### Abstract

Crystal structures of six metamorphic low cordierites with Fe/(Fe + Mg) ranging from 0.07 to 0.42 (atomic) were refined from X-ray data. No evidence of a superstructure was found, confirming that, in chemically intermediate cordierites, Fe and Mg are located on a single site. Although T–O distances remain nearly constant, increased Fe content causes (1) the M site to enlarge, (2) the channels to move apart, and (3) *a* and *b* to increase. In addition, channel rings rotate, change their shape, and move closer together within each channel, causing a decrease in *c*. Difference Fourier maps confirm that channel water is located in a split location near (0,0,1/4). Its orientation is interpreted as being largely controlled by an excess negative charge on O(4) and O(5). The H–O–H plane is oriented nearly parallel to (100) and the H–H vector may either be close to [001] or [010]. Channel cations may be located at several locations at the channel walls in addition to the well-defined site at (0,0,0). Low framework cation-site occupancies are explained by 3–4 percent vacancies that balance for cations in the channel. Vacancies on T(2) and T(5) sites are inversely correlated, and on these sites an increasing number of vacancies produces an enlargement of tetrahedra. Minor differences in mean T–O distances, usually ascribed to Al–Si substitution, may be caused by tetrahedral distortions and vacancies.

### Introduction

Structural aspects of cordierite,  $(\text{Mg}, \text{Fe})_2\text{Al}_4\text{Si}_5\text{O}_{18} \cdot n\text{H}_2\text{O}$ , have recently been the topic of lively discussions. Although the basic cordierite structure (Fig. 1) has been known for some time, intriguing questions have persisted. The present study is based on X-ray refinements made from six cordierites collected from the Bergell region in the Central Alps. These multiple refinements allowed us to observe trends in several structural parameters and to deduce how a number of them are related.

Although cordierite displays a wide range of Fe–Mg substitution, its effect on the cordierite structure has not been systematically examined. Our study fills this need because the six crystals display Fe/(Fe + Mg) values ranging from 0.07 to 0.42 (atomic). Over this compositional range it was found that the cordierite structure adjusts to Fe–Mg substitution in a regular fashion.

A considerable portion of the recent interest in cordierite relates to the channels formed by the stacking of six-membered tetrahedral rings parallel to (001). There is general agreement that the majority

of the minor constituents found in cordierite are located in these channels, although there is discussion about their precise location and orientation (Miyashiro, 1957; Smith and Schreyer, 1960; Schreyer and Yoder, 1964; Gibbs, 1966; Meagher, 1967; Farrell and Newnham, 1967; Tsang and Ghose, 1972; Cohen *et al.*, 1977; Goldman *et al.*, 1977). Our study presents new information concerning the location and orientation of water, possible locations for channel constituents at the channel walls, and evidence that the net positive charge of cations in the channel is balanced by cation site vacancies within the cordierite structural framework.

Cohen *et al.* (1977) presented a new interpretation of Al–Si distribution on cordierite tetrahedral sites. Adjustments in tetrahedral dimensions that we observed as Fe substitutes for Mg in the cordierite structure support their analysis.

After our paper was submitted the reviewers (G. E. Brown and M. Hochella) informed us that they had submitted a paper (Hochella *et al.*, 1979) on heating experiments, which arrived at similar conclusions but on the basis of different observations. Their work complements our study. We modified our manuscript

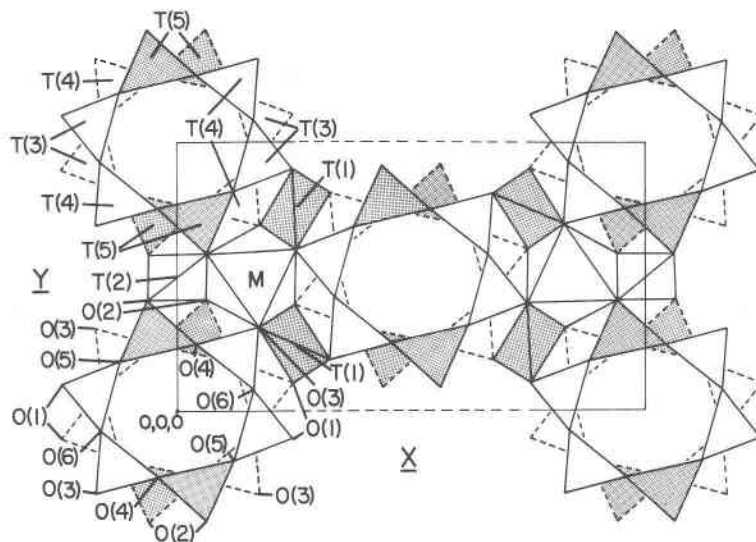


Fig. 1. Structure of low cordierite projected on (001). Aluminum-rich tetrahedra shaded. Symmetrically related polyhedra near dashed unit-cell boundary omitted.

mainly by shortening the review of previous work for which we refer to their paper.

#### Experimental procedures and results

Because of the wide range of metamorphic conditions and the widespread distribution of pelitic rocks of suitable composition, the Bergell region in the Central Alps offers a rare opportunity to collect genetically related metamorphic cordierites of different Fe/(Fe+Mg) content. In this area, increasing Mg content in cordierite has been shown to correspond with increasing Mg bulk composition of the rock and with regional metamorphic conditions of increasing pressure (Wenk *et al.*, 1974).

Six crystals of varying Fe content were selected. Localities and petrographic descriptions of each rock specimen are given in Table 1. The project extended over several years, during which procedures and equipment changed. Several crystals were refined as examples in crystallography courses. The following description may appear exaggerated, but because a number of our interpretations are at the limit of data resolution we thought it worthwhile to specify experimental procedures as completely as possible. Where large crystals were available (Sci 1018, Sci 624), we ground small spheres from fragments; others were picked from petrographic thin sections. Details of the X-ray collection are summarized in Table 2.<sup>1</sup> MoK $\alpha$

<sup>1</sup>Structure factor tables with  $F_0$  and  $F_c$  can be obtained by ordering Document AM-79-120 from the Business Office, Mineralogical Society of America, 2000 Florida Avenue, N. W., Washington, D. C. 20009. Please remit \$1.00 in advance for the microfiche.

radiation with highly oriented graphite as monochromator crystal was used for all samples. A second data set for Sci 1542, using Zr-filtered Mo-radiation, was collected for comparative purposes.

Lattice constants (Table 3 and Fig. 2) were obtained by least-squares refinement, using the diffractometer coordinates of 12–30 medium- to high-angle reflections. Figure 2 shows two specimens with relatively small lattice constants (Sci 1542 and Sci 1104), both measured on the CAD3 diffractometer with monochromator. As is well known, radiation from a graphite monochromator is not strictly monochromatic and there is some ambiguity about its exact wavelength. Therefore, there may be a small sys-

Table 1. Geologic description of analyzed cordierite crystals from the Bergell Alps

Sci 1542	Cordierite-spinel-phlogopite-anthophyllite schist. Inclusion in tonalite. Passo di Mello. Swiss coordinates 776.4/127.8.
Brg 50	Chlorite bearing cordierite-biotite-muscovite schist. Pelitic zone between Tambo nappe and Gruf complex. Alpe Lera Sura. Coordinates 762.6/131.8.
Sci 624	Corundum bearing sapphirine-cordierite-sillimanite-orthopyroxene-garnet-biotite gneiss. Gruf complex. Debris SW Cap Brasca. Coordinates 761.1/125.4.
Sci 1018	Muscovite, apatite and ore bearing cordierite-sillimanite-K feldspar-biotite gneiss. Contact between Bergell granite and Gruf complex. Vallun Trubinasca. Coordinates 764.3/130.2.
Sci 1104	Muscovite and chlorite bearing cordierite-sillimanite-garnet-biotite schist. Inclusion zone in Bergell granite. SW Mte. Rosso. Coordinates 775.1/132.2.
Sci 552	Tourmaline bearing cordierite-andalusite-garnet-biotite-muscovite hornfels. Contact of Bergell granite. Coordinates 773.2/137.9.

Table 2. Details of data collection

	Sci 1542 mono	Sci 1542 filter	Brg 50	Sci 624	Sci 1018	Sci 1104	Sci 552
Diffractometer used	CAD3	CAD3	Picker	Picker	Picker	CAD3	CAD4
Observed reflections	1615	3073	1499	2306	3586	2805	1810
Independent reflections	1465	1907	1499	2306	3395	1635	1810
Reflections used in refinement ( $ F ^2 > 3$ )	1318	1452	1073	1774	2270	1324	1580
R unweighted	0.0290	0.0270	0.0255	0.0269	0.0276	0.0424	0.0261
R weighted	0.0340	0.0325	0.0305	0.0489	0.0323	0.0352	0.0314
Extinction coefficient ( $\times 10^{-6}$ )	8.(2)	6.(1)	0.20(5)	0.18(7)	0.61(4)	-0.15(1.1)	4.1(4)
Linear absorption coefficient $\mu$ ( $\text{cm}^{-1}$ )	9.8		10.3	11.0	14.2	14.9	15.5

tematic error which is also expressed in interatomic distances (compare Fig. 3a-f), and is much less important in interatomic angles (Fig. 3g-i). From all interpretations involving Fe-Mg substitution, averages of Mg- and Fe-rich samples were used. This procedure removes most of the effect of wavelength ambiguity, because Sci 1542 is Mg-rich while Sci 1104 is Fe-rich. Table 3 and Figure 2 also includes the distortion index  $\Delta$  (Miyashiro, 1957) defined as  $\Delta = 2\theta_{131} - (2\theta_{511} + 2\theta_{421} + )/2$ .  $\Delta$  is an index of the deviation of a cordierite from dimensional hexagonality, which can be easily measured on X-ray powder patterns.

Raw intensities were corrected for L-p effects. No absorption correction was applied. Absorption coefficients are given in Table 2. Crystal dimensions ranged from 0.05 to 0.3 mm. When necessary, symmetrically-equivalent reflections in space group *Cccm* were averaged.

Chemical analyses were done with an 8-channel ARL electron microprobe examining for Si, Al, Fe,

Mg, Na, K, Ca, Ti, and Cl (Table 4). The small amounts of material did not allow determinations of H<sub>2</sub>O, CO<sub>2</sub>, or other minor constituents by other analytical methods. If possible, analyses were done on the same crystal fragment used in the structure refinement. Two crystals (Sci 552 and Brg 50) were lost, and analyses refer to an average over several grains in the same thin section. In both cases there was very little variation between grains.

Table 4. Chemical composition and formulae (microprobe analyses). Total iron as FeO. \* = average of several grains in same section

	Sci 1542	Brg 50*	Sci 624	Sci 1018	Sci 1104	Sci 552*
Weight Percent						
SiO <sub>2</sub>	50.6	50.0	50.8	48.6	48.5	48.5
Al <sub>2</sub> O <sub>3</sub>	34.7	34.1	34.5	33.4	33.1	32.8
MgO	12.7	12.0	11.7	8.9	7.7	7.2
FeO	1.69	2.3	3.28	7.5	8.5	9.2
TiO <sub>2</sub>	0.01	<0.01	0	0	<.01	0
CaO	0.02	0.02	<.01	.01	0.02	<.04
Na <sub>2</sub> O	0.14	0.09	.08	.26	.21	.08
K <sub>2</sub> O	0.01	<0.01	0	0	.01	.01
Cl	--	0.015	0	<.01	0	--
Formula						
Si	4.98	5.00	5.00	4.98	5.01	5.03
Al	4.03	4.02	4.00	4.03	4.03	4.01
Mg	1.86	1.79	1.72	1.36	1.19	1.11
Fe	0.14	.19	0.27	0.64	.73	.80
Fe/(Fe+Mg)	0.07	0.10	0.14	0.32	.38	.42

Table 3. Lattice constants and distortion index  $\Delta$  (Miyashiro, 1957). Estimated error of the least significant digit in parentheses

	Sci 1542 mono	Brg 50	Sci 624	Sci 1018	Sci 1104	Sci 552
a	17.044(4)	17.089(3)	17.088(3)	17.114(3)	17.098(4)	17.140(3)
b	9.716(3)	9.737(1)	9.726(1)	9.761(1)	9.741(3)	9.769(2)
c	9.334(2)	9.344(1)	9.335(1)	9.333(1)	9.319(3)	9.321(2)
$\Delta$	0.239	0.248	0.266	0.228	0.249	0.241

Only independent reflections with a net intensity greater than  $3\sigma$  were used in the refinements. Reflections were weighted according to individual standard deviations. Weights of  $W = 1/\sigma$  were assigned in order to avoid overweighting intense reflections, where  $\sigma^2 = \sigma_c^2 + (A \times F_o^2)$ ,  $\sigma_c$  = standard deviation based on counting statistics,  $F_o^2$  = L-p corrected intensity,  $A = 0.0025$ . Using a locally modified version of Busing-Martin-Levy's (1962) least-squares program (NUCLS6), with scattering factors from Cromer and Mann (1968) and anomalous scattering factors for Fe (Cromer, 1965), 93 positional, thermal, extinction, and scale parameters (including occupancies) were refined. The overall isotropic extinction parameter was treated as shown by Zachariasen (1968). It varies from 0. to  $8. \times 10^{-6}$  (Table 2) and probably represents a measure of the perfection of individual crystals.

The refinements proceeded in two phases. In a first phase individual data sets were handled separately as they became available. Refinements on each crystal were carried out until R converged, but there were minor variations in the refinement of oxygen occupancies, the refinement of Fe and Mg and their ratio, the choice of which occupancies were to be held constant, and finally the amounts of Si and Al to be substituted into the tetrahedral sites. The results of the first of these refinements, Sci 1018, have already been reported (Wenk *et al.*, 1974).

In the second phase all refinements were handled in the same manner. Half-ionic scattering factors were used. Oxygens in the tetrahedral framework were held constant at full occupancy. From inspection of interatomic distances from earlier refinements, it was decided to substitute 10 percent Al on

T(2) and 5 percent Si on T(5). Fe-Mg ratios were taken from microprobe analyses. In some cases we also refined them from X-ray intensity data, and results were in close agreement with chemical analyses. The total of Fe+Mg was assumed to be 3.5 percent below that required for full occupancy because of the cation deficiency that has always appeared in previous refinements (see Discussion). Fe was held constant while Mg was allowed to vary. Scattering factors for oxygen and anisotropic thermal parameters were used for both channel sites. With these constraints, refinements for all six crystals converged within two cycles, and results are shown in Tables 5-7. The final positional parameters from these refinements were then used to calculate interatomic distances and angles and served as the basis for Fourier maps. Program ORFFE (Busing *et al.*, 1964) was applied to calculate interatomic distances and angles (Table 8). Errors were determined from both the standard deviations in lattice constants and atomic coordinates.

The results of all the refinements are in overall agreement with previous refinements. In particular, thermal parameters are in close agreement with those of Cohen *et al.* (1977) and, as mentioned by Wenk *et al.* (1974) for Sci 1018, are significantly larger than those reported by Gibbs (1966). The oxygens around the channel [O(4), O(5), and O(6)] show large and more anisotropic thermal parameters than non-channel oxygens. The non-positive definite thermal parameters for the Ch(2) site in Sci 1542 are due to the use of oxygen scattering factors rather than those for smaller cations, such as Na, which actually reside there.

As previously mentioned, we refined two inde-

Table 5. Occupational parameters using half-ionic charge for scattering factors. Ch-atoms are refined as oxygens. Oxygens are fixed at 1.0

	Sci 1542 mono	Sci 1542 filter	Brg 50	Sci 624	Sci 1018	Sci 1104	Sci 552
M-Fe	0.068	0.068	0.090	0.130	0.308	0.366	0.386
M-Mg	0.900(4)	0.886(4)	0.883(4)	0.816(5)	0.626(3)	0.581(5)	0.588(5)
M total	0.968	0.954	0.973	0.946	0.934	0.947	0.974
T(1)-Al	0.962(4)	0.954(4)	0.960(4)	0.964(5)	0.970(2)	0.969(4)	0.978(4)
T(2)-(.9 Si, .1 Al)	0.973(5)	0.960(4)	0.968(5)	0.948(6)	0.982(3)	0.979(6)	0.962(5)
T(3)-Si	0.963(3)	0.960(3)	0.963(4)	0.970(4)	0.966(2)	0.967(4)	0.983(5)
T(4)-Si	0.970(4)	0.958(3)	0.965(4)	0.971(5)	0.960(3)	0.962(4)	0.969(5)
T(5)-(.95 Al, .05 Si)	0.959(4)	0.961(4)	0.950(4)	0.977(5)	0.943(3)	0.954(5)	0.948(5)
Ch(1)	0.74(3)	0.77(4)	0.60(2)	0.96(6)	0.42(1)	0.65(3)	0.60(2)
Ch(2)	0.12(2)	0.08(1)	0.11(1)	0.26(4)	0.16(1)	0.12(1)	0.12(1)
Average cation deficiency (see text)	3.4%	4.2%	3.8%	3.5%	4.1%	3.6%	3.0%

Table 6. Atomic coordinates of cordierites. Estimated error of the least significant digits in parentheses

Cordierites		Sci 1542 monochromator	Sci 1542 filter	Brg 50	Sci 642	Sci 1018	Sci 1104	Sci 552
M	x	.33742(4)	.33739(4)	.33734(5)	.33751(4)	.33734	.33735(3)	.33733(4)
	y = 0							
	z = 1/4							
T(1)	x = 1/4							
	y = 1/4							
	z	.25006(7)	.25008(6)	.25011(8)	.25006(8)	.25011(6)	.25002(10)	.25006(13)
T(2)	x = 0							
	y = 1/2							
	z = 1/4							
T(3)	x	.19252(3)	.19252(3)	.19236(4)	.19234(4)	.19170(3)	.19150(4)	.19135(5)
	y	.07803(6)	.07796(5)	.07803(6)	.07781(6)	.07839(5)	.07853(8)	.07844(9)
	z = 0							
T(4)	x	.13516(3)	.13517(3)	.13526(4)	.13511(4)	.13508(3)	.13506(4)	.13502(5)
	y	-.23731(6)	-.23732(5)	-.23704(6)	-.23714(6)	-.23636(5)	-.23592(8)	-.23589(9)
	z = 0							
T(5)	x	.05083(4)	.05077(4)	.05077(5)	.05059(4)	.05046(3)	.05024(5)	.05032(6)
	y	.30791(6)	.30786(6)	.30795(7)	.30770(7)	.30777(5)	.30751(8)	.30749(10)
	z = 0							
O(1)	x	.24722(6)	.24723(6)	.24695(8)	.24695(7)	.24623(5)	.24584(8)	.24563(9)
	y	-.10301(10)	-.10292(9)	-.10317(11)	-.10288(12)	-.10370(8)	-.10367(13)	-.10374(15)
	z	.35881(11)	.35868(11)	.35876(13)	.35874(13)	.35868(9)	.35849(16)	.35836(17)
O(2)	x	.06220(6)	.06229(6)	.06199(7)	.06208(6)	.06172(4)	.06148(8)	.06144(8)
	y	-.41620(10)	-.41627(10)	-.41601(11)	-.41554(12)	-.41580(8)	-.41534(13)	-.41538(16)
	z	.34910(11)	.34908(10)	.34877(13)	.34870(13)	.34874(9)	.34882(15)	.34922(17)
O(3)	x	-.17326(6)	-.17321(6)	-.17335(7)	-.17323(7)	-.17323(4)	-.17319(8)	-.17322(8)
	y	-.31006(10)	-.31005(10)	-.30949(11)	-.30982(12)	-.30846(8)	-.30796(14)	-.30721(16)
	z	.35854(12)	.35851(11)	.35847(13)	.35824(14)	.35841(9)	.35827(16)	.35803(17)
O(4)	x	.04321(9)	.04305(9)	.04332(11)	.04334(10)	.04332(7)	.04344(12)	.04348(13)
	y	-.24815(16)	-.24824(15)	-.24787(18)	-.24887(19)	-.24703(14)	-.24735(21)	-.24780(27)
	z = 0							
O(5)	x	.12231(9)	.12213(9)	.12217(11)	.12219(10)	.12135(7)	.12149(12)	.12130(14)
	y	.18464(16)	.18479(15)	.18414(17)	.18481(18)	.18391(13)	.18412(21)	.18419(25)
	z = 0							
O(6)	x	.16468(9)	.16474(9)	.16438(11)	.16431(10)	.16390(7)	.16373(12)	.16362(14)
	y	-.07957(15)	-.07956(14)	-.07957(16)	-.07930(17)	-.07889(12)	-.07855(20)	-.07814(24)
	z = 0							
Ch(1)	x = 0							
	y = 0							
	z = .25							
Ch(2)	x = 0							
	y = 0							
	z = 0							

pendently measured data sets from the same crystal (Sci 1542), one with Zr-filtered Mo-radiation and the other using graphite-monochromatized Mo radiation. Of the 92 occupational, positional, thermal, and extinction parameters from the two refinements, 54 are within 1 standard deviation ( $\sigma$ ) of each other, 23 within  $2\sigma$ , 13 within  $3\sigma$ , and 2 within  $4\sigma$ . This nearly normal distribution makes us confident in the quality of X-ray data and the significance of estimated errors. We feel that results from refinements measured

on different diffractometers can be directly and quantitatively compared. In these comparisons Sci 1542 monochromator results were used throughout.

## Discussion

### Framework distortions with Fe-Mg substitution

As Fe substitutes for Mg, the octahedral site enlarges and causes distortions in the structure. One possible effect is an Fe-Mg superstructure in cordier-

Table 7. Anisotropic temperature factors of cordierites ( $\beta_{ij} \times 100$ ). Estimated error of the least significant digits in parentheses

	1542 monochromator	1542 filter	Sci Brq 50	Sci 624	Sci 1018	Sci 1104	Sci 552
M	$\beta_{11}$ .041(2)	.037(3)	.025(3)	.032(2)	.037(1)	.028(2)	.028(2)
	$\beta_{22}$ .121(7)	.120(5)	.112(6)	.109(6)	.125(3)	.118(6)	.127(5)
	$\beta_{33}$ .193(7)	.175(6)	.160(7)	.174(7)	.187(4)	.174(7)	.211(6)
	$\beta_{12} = \beta_{13} = 0$						
	$\beta_{23}$ -.001(5)	-.005(4)	-.007(5)	.008(5)	-.001(3)	.002(5)	-.003(6)
T(1)	$\beta_{11}$ .044(2)	.042(2)	.033(3)	.041(2)	.048(1)	.043(3)	.044(2)
	$\beta_{22}$ .096(6)	.093(5)	.102(6)	.097(6)	.124(4)	.128(8)	.142(8)
	$\beta_{33}$ .104(6)	.100(6)	.110(6)	.111(7)	.110(4)	.110(9)	.143(8)
	$\beta_{12}$ .023(3)	.016(2)	.017(3)	.013(2)	.016(2)	.014(3)	.013(4)
	$\beta_{13} = \beta_{23} = 0$						
T(2)	$\beta_{11}$ .028(3)	.031(3)	.028(4)	.020(2)	.030(2)	.035(3)	.026(3)
	$\beta_{22}$ .115(8)	.098(6)	.113(7)	.091(8)	.142(5)	.128(11)	.126(10)
	$\beta_{33}$ .076(7)	.079(7)	.084(8)	.075(8)	.094(6)	.097(11)	.109(11)
	$\beta_{12} = \beta_{13} = \beta_{23} = 0$						
T(3)	$\beta_{11}$ .031(2)	.031(2)	.029(3)	.030(2)	.030(1)	.031(3)	.029(2)
	$\beta_{22}$ .069(6)	.076(4)	.073(5)	.072(5)	.085(4)	.090(8)	.102(8)
	$\beta_{33}$ .102(6)	.093(5)	.098(6)	.101(6)	.104(4)	.096(9)	.140(8)
	$\beta_{12}$ .004(2)	.001(2)	.000(3)	.008(2)	.003(2)	.003(3)	.005(3)
	$\beta_{13} = \beta_{23} = 0$						
T(4)	$\beta_{11}$ .025(2)	.033(2)	.021(3)	.025(2)	.028(1)	.027(2)	.023(2)
	$\beta_{22}$ .090(6)	.083(5)	.089(6)	.090(5)	.093(4)	.096(8)	.122(8)
	$\beta_{33}$ .099(5)	.098(5)	.102(6)	.104(6)	.096(4)	.089(8)	.124(8)
	$\beta_{12}$ -.005(2)	-.007(2)	-.006(3)	-.009(2)	-.008(2)	-.011(3)	-.009(3)
	$\beta_{13} = \beta_{23} = 0$						
T(5)	$\beta_{11}$ .028(2)	.033(2)	.019(3)	.029(2)	.024(1)	.024(3)	.016(3)
	$\beta_{22}$ .085(6)	.099(5)	.096(6)	.109(6)	.099(4)	.133(9)	.117(9)
	$\beta_{33}$ .110(6)	.106(6)	.099(7)	.115(7)	.097(5)	.096(10)	.126(10)
	$\beta_{12}$ .008(3)	.006(2)	.008(3)	.006(2)	.006(2)	.009(4)	.007(4)
	$\beta_{13} = \beta_{23} = 0$						
O(1)	$\beta_{11}$ .078(3)	.088(4)	.082(5)	.074(3)	.083(2)	.083(4)	.074(4)
	$\beta_{22}$ .155(10)	.154(8)	.171(9)	.167(9)	.171(7)	.175(14)	.191(13)
	$\beta_{33}$ .176(10)	.172(9)	.169(10)	.159(10)	.176(7)	.187(15)	.206(14)
	$\beta_{12}$ -.016(4)	-.011(4)	-.007(6)	-.018(4)	-.008(3)	.000(6)	-.006(6)
	$\beta_{13}$ .032(5)	.030(4)	.025(7)	.045(5)	.037(3)	.038(7)	.035(7)
	$\beta_{23}$ -.025(8)	-.026(7)	-.019(8)	-.027(8)	-.019(6)	-.012(12)	-.005(12)
O(2)	$\beta_{11}$ .054(3)	.059(3)	.058(5)	.049(3)	.059(2)	.063(4)	.054(4)
	$\beta_{22}$ .232(10)	.221(8)	.227(9)	.215(10)	.239(7)	.246(13)	.240(13)
	$\beta_{33}$ .184(10)	.185(9)	.193(11)	.179(11)	.184(7)	.170(15)	.223(15)
	$\beta_{12}$ -.014(5)	-.010(4)	-.010(6)	-.013(4)	-.012(3)	-.017(6)	-.015(6)
	$\beta_{13}$ .004(4)	.011(4)	.001(6)	-.003(4)	.006(3)	.003(7)	.013(7)
	$\beta_{23}$ -.057(8)	-.057(7)	-.067(8)	-.088(8)	-.075(6)	-.067(12)	-.086(13)
O(3)	$\beta_{11}$ .067(3)	.076(3)	.062(4)	.059(3)	.067(2)	.059(4)	.059(4)
	$\beta_{22}$ .203(10)	.193(8)	.214(9)	.200(10)	.221(7)	.224(14)	.228(13)
	$\beta_{33}$ .179(10)	.185(10)	.185(11)	.185(11)	.171(7)	.190(16)	.212(15)
	$\beta_{12}$ .023(5)	.012(4)	.022(6)	.015(4)	.013(3)	.019(6)	.019(6)
	$\beta_{13}$ -.024(4)	-.030(4)	-.018(6)	-.023(5)	-.025(3)	-.294(6)	-.017(6)
	$\beta_{23}$ -.026(8)	-.047(7)	-.043(9)	-.053(8)	-.046(6)	-.047(12)	-.036(13)
O(4)	$\beta_{11}$ .051(5)	.053(6)	.058(7)	.035(4)	.044(3)	.052(6)	.036(6)
	$\beta_{22}$ .299(16)	.334(14)	.338(16)	.332(16)	.365(12)	.358(23)	.383(24)
	$\beta_{33}$ .371(17)	.339(16)	.388(19)	.351(18)	.384(14)	.415(26)	.446(27)
	$\beta_{12}$ -.011(7)	-.015(6)	-.010(9)	-.027(6)	-.018(5)	-.012(10)	-.023(11)
	$\beta_{13} = \beta_{23} = 0$						
O(5)	$\beta_{11}$ .074(5)	.069(5)	.090(7)	.065(5)	.087(3)	.088(7)	.079(7)
	$\beta_{22}$ .239(16)	.237(13)	.230(14)	.219(15)	.263(11)	.261(21)	.259(22)
	$\beta_{33}$ .361(18)	.373(17)	.374(19)	.383(19)	.375(14)	.366(28)	.409(28)
	$\beta_{12}$ .047(7)	.063(6)	.045(9)	.058(7)	.077(5)	.064(9)	.056(11)
	$\beta_{13} = \beta_{23} = 0$						
O(6)	$\beta_{11}$ .091(5)	.102(5)	.099(7)	.089(5)	.102(4)	.096(7)	.084(7)
	$\beta_{22}$ .151(15)	.127(11)	.143(13)	.118(13)	.136(9)	.138(20)	.175(19)
	$\beta_{33}$ .415(17)	.387(16)	.378(18)	.388(18)	.398(14)	.355(25)	.394(26)
	$\beta_{12}$ -.027(7)	-.026(6)	-.031(9)	-.037(7)	-.043(5)	-.034(10)	-.017(10)
	$\beta_{13} = \beta_{23} = 0$						
Ch(1)	$\beta_{11}$ 5.1(4)	5.0(3)	3.2(2)	22.0(2)	.59(2)	2.8(2)	1.8(2)
	$\beta_{22}$ 2.6(3)	2.8(3)	2.4(3)	1.8(3)	1.6(2)	2.4(3)	2.5(3)
	$\beta_{33}$ 1.1(2)	1.2(2)	1.7(2)	7.5(12)	.82(8)	1.7(2)	1.9(3)
	$\beta_{12} = \beta_{13} = \beta_{23} = 0$						
Ch(2)	$\beta_{11}$ .1(1)	-.1(1)	.2(1)	1.5(4)	.01(1)	.03(8)	.2(1)
	$\beta_{22}$ -.1(3)	-.4(1)	.6(3)	2.2(9)	.26(6)	.3(3)	.1(2)
	$\beta_{33}$ 51(20)	32(7)	1.0(4)	5.7(17)	1.1(2)	.4(3)	.9(5)
	$\beta_{12}$ .2(2)	.23(7)	.2(2)	.1(4)	-.05(3)	.0(1)	.0(2)
	$\beta_{13} = \beta_{23} = 0$						

Table 8. Interatomic distances and angles of cordierites. Estimated standard errors in parentheses. \* = occurs twice. \*\* = occurs four times. S = shared edges

	1542 mono	1542 filter	Brg 50	624	1018	1104	552
<b>M-Oc tetrahedron</b>							
M-O(1)*	2.0968(11)	2.0953(11)	2.1043(13)	2.1040(12)	2.1177(8)	2.1189(14)	2.1255(16)
M-O(2)*	2.1034(12)	2.1074(12)	2.1166(13)	2.1138(12)	2.1235(8)	2.1261(14)	2.1327(16)
M-O(3)*	2.1131(11)	2.1129(11)	2.1217(11)	2.1158(12)	2.1335(8)	2.1330(14)	2.1433(16)
Average	2.1061	2.1052	2.1142	2.1112	2.1249	2.1260	2.1338
O(1)-O(1)	2.8518(21)	2.8489(21)	2.8579(23)	2.8509(24)	2.8589(16)	2.8543(26)	2.8615(30)
O(1)-O(2)*	3.2548(16)	3.2530(17)	3.2716(19)	3.2696(16)	3.2936(12)	3.3008(20)	3.3131(21)
O(1)-O(3)*S	2.5819(15)	2.5813(15)	2.5380(17)	2.5854(16)	2.5962(11)	2.5958(19)	2.5959(21)
O(1)-O(3)**	3.1526(17)	3.1521(16)	3.1672(16)	3.1601(17)	3.1945(11)	3.1958(20)	3.2135(22)
O(2)-O(2)S	2.4646(20)	2.4635(20)	2.4662(22)	2.4690(23)	2.4695(16)	2.4723(27)	2.4808(31)
O(2)-O(3)*	2.8987(15)	2.8972(15)	2.9064(17)	2.8978(17)	2.9116(12)	2.9097(20)	2.9186(21)
O(2)-O(3)**	3.2657(16)	3.2638(16)	3.2823(16)	3.2790(16)	3.3006(11)	3.3045(19)	3.3199(22)
Average	2.9687	2.9673	2.9796	2.9753	2.9935	2.9950	3.0060
O(1)-M-O(1)	85.69(6)	85.66(6)	85.54(7)	85.29(7)	85.17(5)	84.81(8)	84.62(9)
O(1)-M-O(2)*	101.42(4)	101.44(4)	101.63(5)	101.65(5)	101.30(3)	102.03(5)	102.16(6)
O(1)-M-O(3)**	75.65(4)	75.67(4)	75.53(5)	75.57(5)	75.23(3)	75.25(5)	75.04(6)
O(1)-M-O(3)*S	96.98(4)	97.01(4)	97.09(5)	96.99(5)	97.43(3)	97.46(5)	97.66(6)
O(2)-M-O(2)	71.53(6)	71.54(6)	71.27(7)	71.47(6)	71.11(4)	71.10(8)	71.13(8)
O(2)-M-O(3)*	86.73(4)	86.71(4)	86.59(5)	86.49(5)	86.31(3)	86.19(5)	86.09(6)
O(2)-M-O(3)**	101.35(4)	101.31(4)	101.51(5)	101.66(5)	101.67(3)	101.77(6)	101.86(6)
Average	90.12	90.12	90.13	90.12	90.12	90.12	90.12
<b>T(1) Tetrahedron</b>							
T(1)-O(1)*	1.7535(11)	1.7535(11)	1.7554(12)	1.7556(12)	1.7534(9)	1.7492(15)	1.7516(17)
T(1)-O(3)*	1.7540(11)	1.7543(11)	1.7539(13)	1.7549(13)	1.7531(9)	1.7496(15)	1.7485(17)
Average	1.7538	1.7539	1.7547	1.7553	1.7533	1.7494	1.7501
O(1)-O(1)	2.8579(21)	2.8595(2)	2.8612(21)	2.8640(23)	2.8668(16)	2.8580(28)	2.8617(31)
O(1)-O(3)*S	2.5819(15)	2.5813(15)	2.5880(17)	2.5854(16)	2.5962(11)	2.5958(19)	2.5999(21)
O(1)-O(3)**	3.1228(15)	3.1227(15)	3.1206(16)	3.1212(17)	3.1082(11)	3.0958(20)	3.0918(22)
O(3)-O(3)	2.8644(21)	2.8659(22)	2.8644(25)	2.8702(23)	2.8650(16)	2.8590(27)	2.8596(29)
Average	2.8553	2.8557	2.8571	2.8579	2.8568	2.8500	2.8508
O(1)-T-O(1)	109.16(8)	109.25(8)	109.17(8)	109.31(9)	109.23(6)	109.36(11)	109.53(12)
O(1)-T-O(3)*	94.80(5)	94.76(5)	95.03(5)	94.87(5)	95.53(4)	95.79(6)	95.94(7)
O(1)-T-O(3)**	125.83(5)	125.80(5)	125.55(6)	125.52(5)	124.85(4)	124.46(6)	124.10(7)
O(3)-T-O(3)	109.48(8)	109.54(8)	109.48(9)	109.73(9)	109.59(6)	109.58(11)	109.72(12)
Average	109.98	109.99	109.97	109.97	109.93	109.91	109.89
<b>T(2) Tetrahedron</b>							
T(2)-O(2)**	1.6256(10)	1.6262(10)	1.6256(12)	1.6276(11)	1.6249(8)	1.6226(14)	1.6272(15)
Average	1.6256	1.6262	1.6256	1.6276	1.6249	1.6226	1.6272
O(2)-O(2)*S	2.4646(20)	2.4635(20)	2.4662(22)	2.4690(23)	2.4695(16)	2.4723(27)	2.4808(31)
O(2)-O(2)**	2.6736(20)	2.6751(21)	2.6766(24)	2.6834(22)	2.6765(15)	2.6724(26)	2.6777(30)
O(2)-O(2)*	2.8141(21)	2.8161(21)	2.8099(25)	2.8102(23)	2.8034(16)	2.7950(28)	2.8031(31)
Average	2.6508	2.6516	2.6521	2.6542	2.6498	2.6505	2.6558
O(2)-T-O(2)*	98.59(7)	98.48(7)	98.67(8)	98.66(8)	98.91(5)	99.25(9)	99.34(10)
O(2)-T-O(2)**	110.64(7)	110.60(7)	110.82(8)	111.04(8)	110.90(6)	110.84(10)	110.73(11)
O(2)-T-O(2)*	119.89(8)	119.96(7)	119.59(8)	119.37(8)	119.23(6)	118.91(10)	118.93(11)
Average	109.71	109.71	109.69	109.69	109.68	109.67	109.67
<b>T(3) Tetrahedron</b>							
T(3)-O(1)*	1.6324(11)	1.6335(11)	1.6346(13)	1.6337(12)	1.6345(8)	1.6317(15)	1.6339(16)
T(3)-O(5)	1.5828(16)	1.5864(15)	1.5832(19)	1.5876(18)	1.5844(12)	1.5783(20)	1.5840(24)
T(3)-O(6)	1.6030(16)	1.6019(16)	1.6073(17)	1.6015(17)	1.6073(12)	1.6020(21)	1.6017(24)
Average	1.6127	1.6138	1.6149	1.6141	1.6152	1.6109	1.6134
O(1)-O(1)	2.6357(18)	2.6382(18)	2.6395(20)	2.6373(19)	2.6380(12)	2.6376(22)	2.6405(25)
O(1)-O(5)**	2.6265(17)	2.6304(17)	2.6288(20)	2.6304(18)	2.6306(13)	2.6218(22)	2.6272(26)
O(1)-O(6)**	2.6197(17)	2.6192(16)	2.6265(18)	2.6217(18)	2.6270(12)	2.6192(21)	2.6221(26)
O(5)-O(6)	2.6667(22)	2.6690(21)	2.6671(23)	2.6680(24)	2.6666(17)	2.6586(28)	2.6634(34)
Average	2.6325	2.6344	2.6362	2.6349	2.6366	2.6297	2.6338
O(1)-T-O(1)	107.67(5)	107.71(5)	107.68(5)	107.64(6)	107.60(4)	107.85(8)	107.81(8)
O(1)-T-O(5)**	109.54(5)	109.55(5)	109.56(6)	109.47(6)	109.61(4)	109.52(7)	109.45(8)
O(1)-T-O(6)**	108.13(5)	108.09(5)	108.23(6)	108.26(6)	108.26(4)	108.19(7)	108.27(8)
O(5)-T-O(6)	113.66(9)	113.68(9)	113.43(10)	113.56(11)	113.33(7)	113.43(11)	113.44(13)
Average	109.45	109.45	109.45	109.44	109.45	109.45	109.45
<b>T(4) Tetrahedron</b>							
T(4)-O(3)*	1.6324(11)	1.6321(11)	1.6341(13)	1.6357(12)	1.6334(8)	1.6316(15)	1.6326(16)
T(4)-O(4)	1.5708(16)	1.5737(17)	1.5746(20)	1.5723(18)	1.5738(13)	1.5703(21)	1.5734(23)
T(4)-O(6)	1.6131(16)	1.6136(15)	1.6120(17)	1.6143(17)	1.6142(12)	1.6095(21)	1.6172(26)
Average	1.6122	1.6129	1.6137	1.6145	1.6137	1.6108	1.6140
O(3)-O(3)	2.6408(17)	2.6413(17)	2.6447(20)	2.6468(20)	2.6431(14)	2.6417(24)	2.6468(26)
O(3)-O(4)*	2.6493(18)	2.6508(18)	2.6546(21)	2.6513(19)	2.6549(13)	2.6485(23)	2.6520(25)
O(3)-O(6)**	2.6038(17)	2.6039(17)	2.6047(18)	2.6081(19)	2.6064(13)	2.6009(23)	2.6050(26)
O(4)-O(6)	2.6399(21)	2.6436(21)	2.6392(26)	2.6445(24)	2.6367(17)	2.6332(29)	2.6434(35)
Average	2.6312	2.6324	2.6338	2.6350	2.6337	2.6290	2.6340
O(3)-T-O(3)	107.97(5)	108.03(5)	108.04(6)	108.01(6)	108.01(4)	108.10(7)	108.31(8)
O(3)-T-O(4)*	111.58(5)	111.54(5)	111.63(6)	111.46(6)	111.73(4)	111.60(7)	111.61(8)
O(3)-T-O(6)**	106.69(5)	106.69(5)	106.72(6)	106.73(6)	106.75(4)	106.73(7)	106.57(8)
O(4)-T-O(6)	112.02(9)	112.07(9)	111.82(10)	112.17(10)	111.59(7)	111.80(11)	111.89(14)
Average	109.42	109.43	109.43	109.43	109.43	109.43	109.43
<b>T(5) Tetrahedron</b>							
T(5)-O(2)*	1.7687(11)	1.7698(11)	1.7722(12)	1.7702(12)	1.7726(9)	1.7679(15)	1.7671(17)
T(5)-O(4)	1.7047(17)	1.7077(17)	1.7110(20)	1.7040(18)	1.7111(13)	1.7055(21)	1.7107(20)
T(5)-O(5)	1.7083(17)	1.7058(16)	1.7151(19)	1.7105(18)	1.7128(13)	1.7113(21)	1.7119(24)
Average	1.7376	1.7385	1.7426	1.7387	1.7423	1.7385	1.7391
O(2)-O(2)	2.8169(18)	2.8173(18)	2.8262(20)	2.8249(19)	2.8235(12)	2.8179(22)	2.8110(30)
O(2)-O(4)*	2.8067(17)	2.8069(17)	2.8135(20)	2.8050(18)	2.8175(13)	2.8073(22)	2.8088(31)
O(2)-O(5)**	2.8451(17)	2.8431(17)	2.8551(19)	2.8437(19)	2.8563(13)	2.8479(22)	2.8510(26)
O(4)-O(5)	2.8877(22)	2.8821(22)	2.8952(27)	2.8964(24)	2.8848(17)	2.8864(28)	2.8918(33)
Average	2.8347	2.8329	2.8431	2.8365	2.8427	2.8358	2.8371
O(2)-T-O(2)	105.56(4)	105.49(5)	105.76(6)	105.86(5)	105.58(4)	105.68(7)	105.38(8)
O(2)-T-O(4)*	107.80(5)	107.88(5)	107.74(6)	107.67(6)	107.94(4)	107.83(6)	107.75(8)
O(2)-T-O(5)**	109.81(5)	109.76(5)	109.90(6)	109.56(6)	110.06(4)	109.87(6)	110.06(8)
O(4)-T-O(5)	115.58(9)	115.57(8)	115.35(10)	116.04(10)	114.83(7)	115.29(11)	115.35(13)
Average	109.39	109.39	109.40	109.39	109.40	109.40	109.39

ites of intermediate composition. However, we could not find any indication for this even on very strongly exposed X-ray photographs, indicating that Fe and Mg are distributed randomly on the same structural site.

Adjustments to the enlarged octahedral site are expressed in changes of the cell dimensions and of interatomic distances and angles. With increasing Fe content,  $a$  and  $b$  increase while  $c$  contracts slightly (Fig. 2). The average M–O interatomic distance varies almost linearly with Fe (Fig. 3a), in accordance with other FeMg silicates (e.g. olivines, Wenk and Raymond, 1973). While there is little effect on the average size of tetrahedra (Table 8), there are systematic distortions in the tetrahedral framework and in the shape of non-channel tetrahedra T(1) and T(2) (Fig. 3e,f,h,i). In addition to size, the shape of the octahedron changes. This is indicated by octahedral O–O distances and O–M–O angles, which vary at different rates (Fig. 3d,g). Note that  $z$  atomic coordinates are almost constant while there is considerable variation in  $x$  and  $y$ . Similarly,  $c$  changes at a much slower rate than either  $a$  or  $b$ . These are indications that distortions are mainly confined to the  $xy$  plane.

To study the framework distortion we plotted the relative shift of each atom in the  $xy$  projection as Fe substitutes for Mg. As is clear from Figure 4, we are at the limit of resolution and a statistical approach may improve it. Since three samples are Mg-rich (the average of Sci 1542, Brg 50, and Sci 624 is 10 percent Fe) and three are Fe-rich (Sci 1018, Sci 1104, and Sci 552 average to 37 percent Fe), we chose to average each group by constructing the centers of triangles. Figure 4 gives a typical example of a good fit (Fig. 4a), an average variation (Fig. 4b), and a poor fit (Fig. 4c). The connecting vector between the two centers characterizes the shift and corresponds to a substitution of 0.27 Fe/(Fe+Mg). These migration vectors for all atoms are plotted in Figure 5a, with their lengths exaggerated 100 times.

A regular pattern emerges from these plots. As vectors for M, T(1), and T(2) point away from the ring, indicating an increase in the unit-cell size, atoms in the ring at  $z = 0$  perform a counterclockwise rotation. By symmetry, the ring at  $z = 0.5$  has a clockwise rotation (Fig. 5b). This rotation allows M–O distances to increase. There is some variation in these shifts which may be due to scatter in the data or, more likely, to a small regular distortion of the ring. We calculate an average rotation of  $0.14^\circ$  around the channel axis. Hochella *et al.* (1979) have independently shown that the heating of Mg-cordier-

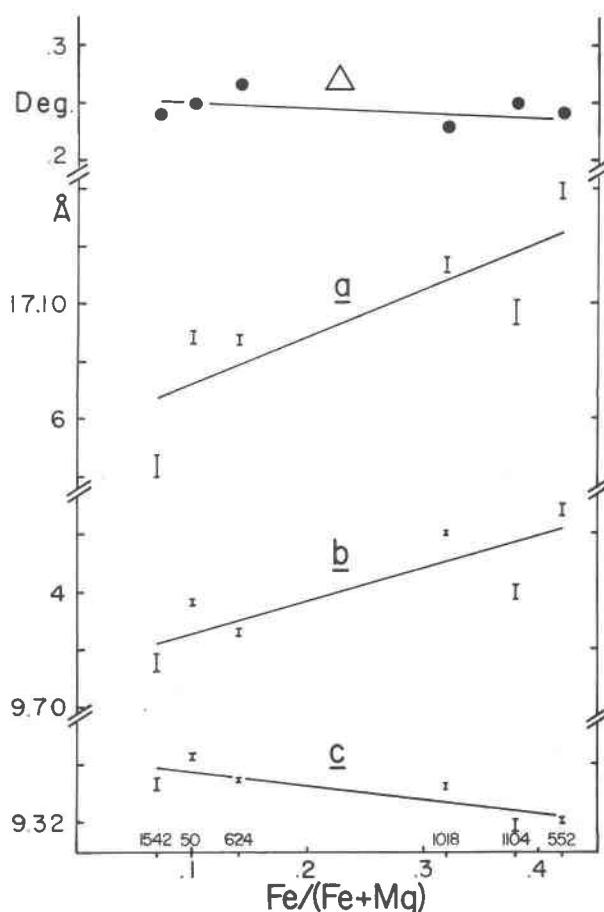


Fig. 2. Variation of lattice constants and distortion index  $\Delta$  with Fe–Mg content. Bars represent  $\pm$  one standard deviation.

ite causes a channel-ring rotation similar to the one observed here. Also, ring rotations have been observed in heating experiments with beryl performed by Brown and Mills (1980).

The possibility of a small regular distortion of the ring was evaluated by removing the  $0.14^\circ$  rotational component from the displacement vectors of ring atoms. The resulting vectors (dashed arrows in Fig. 5a) indicate a slight contraction of the ring parallel to  $x$  and an elongation parallel to  $y$ . Since the magnitude of ring distortion is small relative to that of the rotation, we will simplify the following discussion by temporarily ignoring it.

Figure 5c illustrates how the cordierite structure adjusts to substitution of Fe for Mg and the resulting increased M–O distances. It is accomplished first by channels moving apart, causing increases in lattice constants  $a$  and  $b$ . Secondly, the channel rings rotate, thereby moving the three-coordinated oxygens further from the M site. However, not only does the

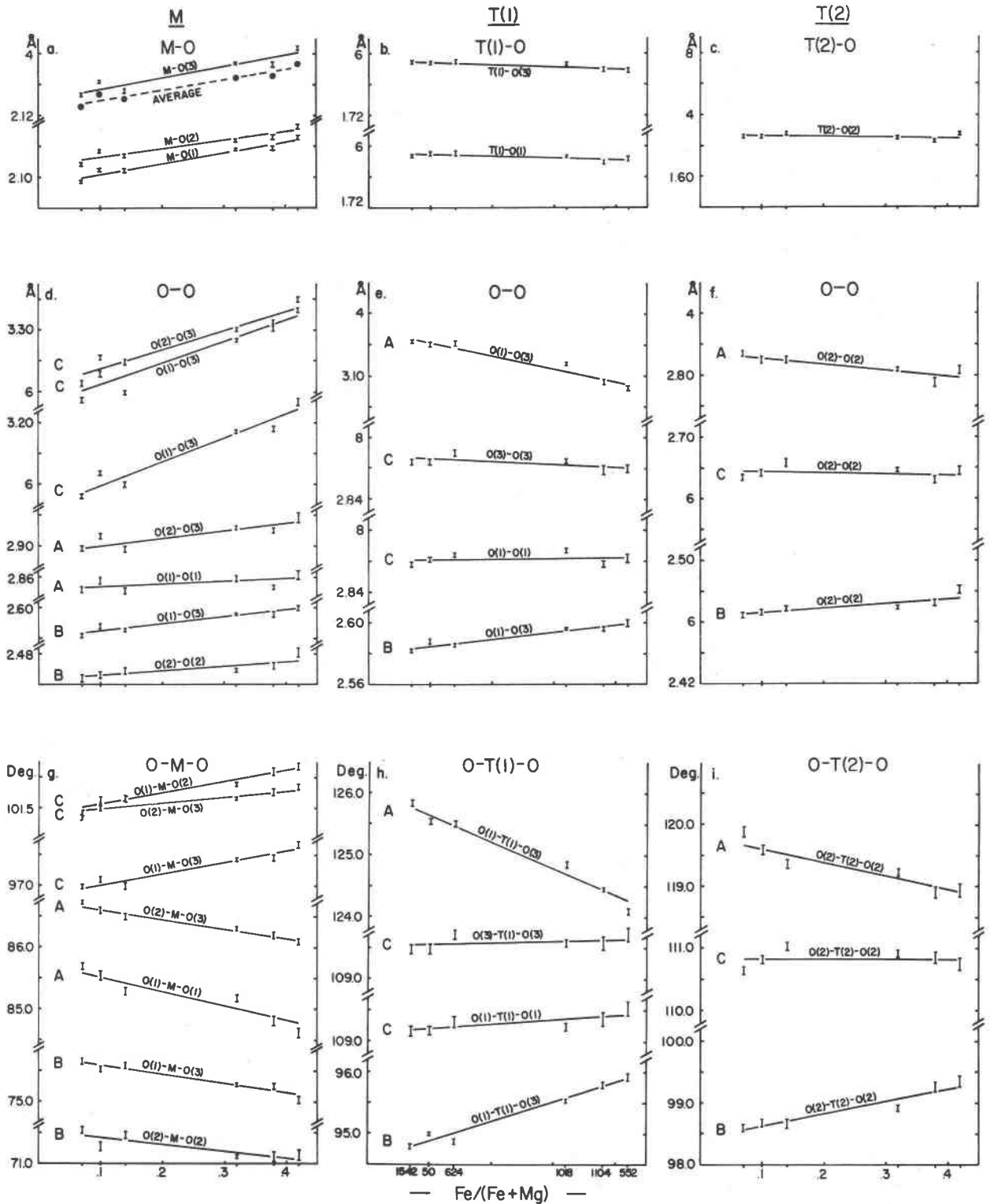


Fig. 3. Variation of octahedral and T(1) and T(2) tetrahedral interatomic distances and angles with Fe-Mg content. Bars represent  $\pm$  one standard deviation. A—distances and angles between rings at successive levels of the same channel; B—distances and angles between rings at successive levels of adjacent channels; C—distances and angles between the same level of adjacent channels.

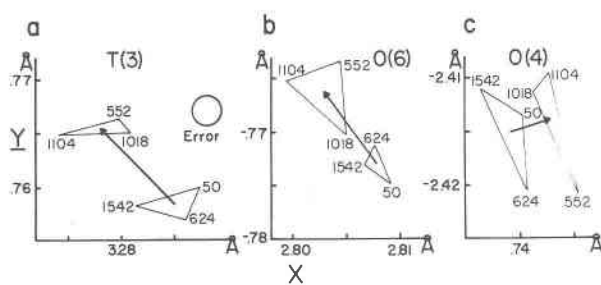


Fig. 4. Derivation of site migration vectors in a (001) projection. Triangle centers are the average of Fe-rich and Mg-rich samples; the arrow represents the vector connecting them. Error circle has radius of approximately one standard deviation in atomic position. (a) Good fit; (b) typical fit; (c) poor fit.

structure have to accommodate increased M–O distances, but it must keep the T(1)–O and T(2)–O distances roughly constant as the channels move apart. As Figure 5c indicates, the channel-ring rotation helps to accomplish this because it causes the three-coordinated oxygens to move towards the T(1) and T(2) sites. Also, T(1)–O and T(2)–O distances are maintained by the rings moving closer together within each channel. This causes the decrease in  $c$ .

Figures 3b and 3c show that T(1)–O and T(2)–O distances actually decrease slightly as Fe/(Fe+Mg) increases. This change, although small, seems significant, because all three distances decrease by a similar amount and this is exactly what we would expect from decreasing distortion of the T(1) and T(2) tetrahedra (Fig. 3e, f, h, i). Cohen *et al.* (1977) show that a decrease in tetrahedral distortion should be accompanied by a decrease in T–O distances. We will elaborate on this point in the section on Al–Si distribution.

The variety of slopes in Figure 3 show that within a given polyhedron the different interatomic distances and angles undergo different changes. We suggest that this entire assortment of changes is explained by the structural accommodation to Fe–Mg substitution described above. A similar conclusion was reached by Hochella *et al.* (1979) to explain structural changes in Mg cordierite caused by heating. M–O and T–O distances have already been discussed. O–O distances and corresponding angles may be grouped according to their relationship with the channel rings. They either join rings located at successive levels of the same channel (graphs labeled A in Fig. 3), rings located at successive levels of adjacent channels (labeled B), or rings located at the same level of adjacent channels (labeled C). It is immediately apparent that within the octahedron or ei-

ther tetrahedron, distances and angles grouped in this manner all have a similar size and undergo a similar change as Fe/(Fe+Mg) increases. Furthermore, these changes can easily be explained by the structural accommodation to an enlarged M site already described. Understanding the change in a given group of distances or angles requires consideration of the following factors: enlarged M–O distances, channels moving apart, channel-ring rotation, and the contraction of the distance between rings within each channel. For example, all these factors should cause the three octahedral distances and corresponding angles between the same levels of adjacent channels to increase. Sharp increases are documented by Figures 3d and 3g.

The effect of the distortion of the channel ring that we have so far ignored is to enhance the effect of the structural adjustments to increasing Fe/(Fe+Mg) discussed above. The elongation parallel to  $y$  helps to maintain the T(2)–O distances while the shortening parallel to  $x$  further removes distortion from the T(1)

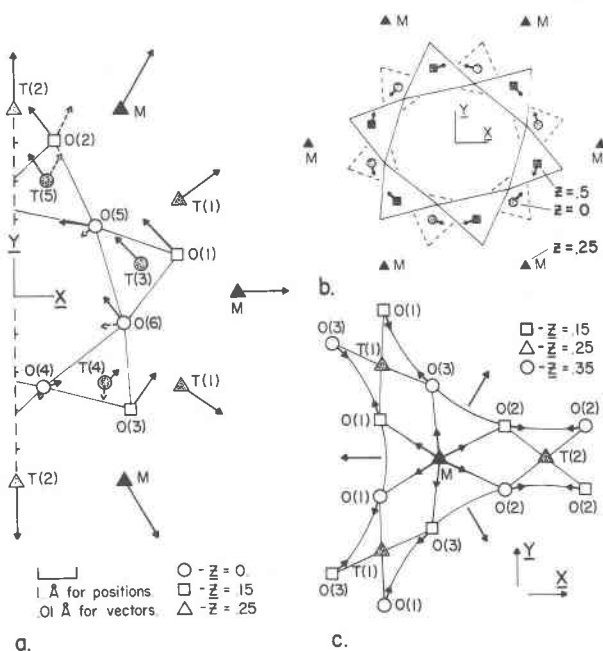


Fig. 5. Site migration in  $xy$  projection as Fe/(Fe+Mg) increases from 10 to 37 percent. T sites stippled, oxygen sites open, M sites solid. (a) Migration vectors (solid arrows) and radial component of migration vectors of ring atoms after removing  $0.14^\circ$  ring rotation (dashed arrows, omitted where insignificantly small). Vectors exaggerated 100 times. (b) Schematic drawing illustrating rotation of successive rings. (c) Schematic drawing illustrating framework adjustments due to enlargement of the M site.

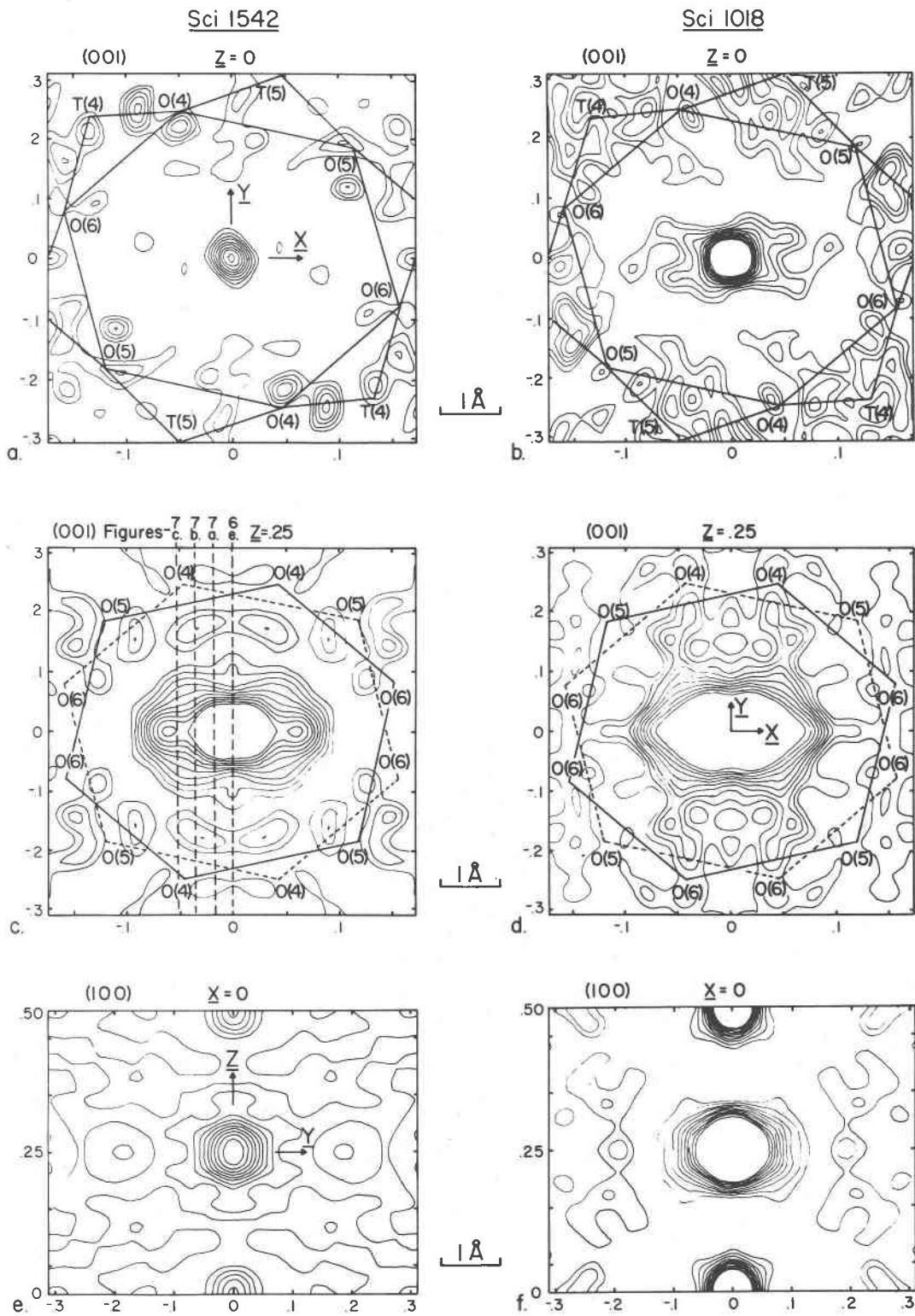


Fig. 6. Difference Fourier sections through channel. Channel sites removed for calculation. Negative contours omitted. Labeled axes give atomic coordinates. Channel rings superimposed on (001) sections. (c) gives locations of serial (100) sections for Sci 1542 in Fig. 6c and 7a-c.

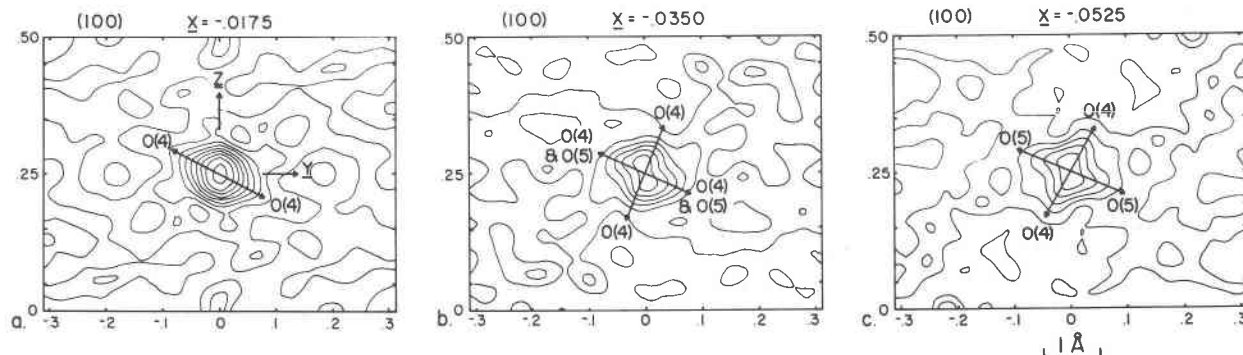


Fig. 7. Serial (100) difference Fourier sections through channel  $H_2O$ . Channel sites removed from calculation. Negative contours omitted. Electron densities on same scale as Fig. 6e. Arrows indicate polarization of H atoms by ring oxygens.

tetrahedron. The change in shape of the channel has only a small effect on the distortion index  $\Delta$  (Fig. 2). It should be noted that  $a$  and  $b$  are much more sensitive to the iron content than is the distortion index and therefore are better determinative parameters.

In summary, the increase in M–O distances with increasing Fe/(Fe+Mg) forces the channels apart, increasing  $a$  and  $b$ . It causes the tetrahedral channel rings to rotate and also to become more hexagonal in shape. The rotation and shape change of the rings, coupled with the decrease in  $c$  caused by the contraction of the distance between rings, allows the T(1)–O and T(2)–O distances to remain nearly constant. All other changes in dimensions can be explained as a consequence of this basic mechanism.

#### Channel constituents

An aspect of the cordierite structure which has received much attention is the location and orientation of water. In our study we relied on difference Fourier maps which have channel atoms removed for the calculation (Figs. 6 and 7). We illustrate results for two samples: Sci 1542 (Mg-rich) and Sci 1018 (Fe-rich). A broad asymmetric peak is displayed in  $xy\frac{1}{2}$  and  $0yz$  sections (Fig. 6c–f), which is explained by the split location for the water oxygen ( $x = 0.027$ ,  $y = 0$ ,  $z = \frac{1}{2}$ ) proposed by Cohen *et al.* (1977). We unsuccessfully attempted to refine the water oxygen as a split atom. Looking at the  $xy\frac{1}{2}$  section alone one could visualize a water molecule lying in this plane. However, we constructed a series of difference Fourier sections normal to [100] through the water location (Figs. 6e and 7, position of each section indicated on Fig. 6c), which show an asymmetry that can most easily be explained by having the H–O–H plane nearly parallel to (100). This disagrees with Cohen *et al.* but is in agreement with the conclusions of Farrell

and Newnham (1967), Tsang and Ghose (1972), Goldman *et al.* (1977), and Hochella *et al.* (1979).

Orientation of the water appears to be controlled by the O(4) and O(5) oxygens, which have a residual negative charge because they are doubly coordinated with Al and Si. The section through the channel center (Fig. 6e) is highly symmetrical because it is influenced equally by the water molecules at both split locations. But moving away from the center ( $x = -0.0175$ , Fig. 7a) an asymmetric bulge develops. Comparing with the structure (Fig. 6c), we find that it is pointing towards O(4) at  $x = 0.043$ ,  $y = -0.248$ ,  $z = 0$  and the symmetric equivalent at  $x = 0.043$ ,  $y = 0.248$ ,  $z = \frac{1}{2}$ . We interpret this as being caused by the polarization of H towards these O(4) atom locations. Further out ( $x = -0.035$ , Fig. 7b) is a section which probably goes nearly through the center of the loosely defined water oxygen location. Two new bulges appear which are pointing towards O(4) locations at  $x = -0.043$ ,  $y = 0.248$ ,  $z = 0$  and  $x = -0.043$ ,  $y = -0.248$ ,  $z = \frac{1}{2}$ . The bulge previously discussed is now interpreted as a superposition of the elongation towards O(4) (Fig. 7a) and an elongation towards O(5) at  $x = -0.122$ ,  $y = -0.185$ ,  $z = 0$  and  $x = -0.122$ ,  $y = 0.185$ ,  $z = \frac{1}{2}$ . Still further out ( $x = -0.0525$ , Fig. 7c) the bulges are caused by polarizations towards O(4) and O(5) as indicated.

Figure 7 is consistent with the H–H water vector oriented nearly parallel to either [001] or [010]. Goldman *et al.* (1977) suggested that the choice between these orientations may be determined by the channel constituents at the origin. Hochella *et al.* (1979) suggest that the H–H vector is inclined at  $19^\circ$  to [001]. Our data are consistent with this interpretation.

The channel site at (0, 0, 0) is smaller and more symmetrical than the one in the neighborhood of (0, 0,  $\frac{1}{2}$ ) (Fig. 6a–d). In Sci 1542 it even refined to nega-

tive temperature factors. Note that there is little correlation between the refined occupancy of this site and any of the minor constituents in the microprobe data. One reason for this is that we may be beyond the limit of resolution for both the occupancy and microprobe data. Another possibility, suggested by Goldman *et al.* (1977), is that minor cation constituents may be diffusely distributed over several other locations in the channel. In fact, difference Fourier plots all show rather high positive anomalies at the channel walls at both  $z = 0$  (Fig. 6a, b) and  $z = \frac{1}{4}$  (Fig. 6c, d).

#### Vacancies on tetrahedral and octahedral sites

A trend observed in the refinements of all samples is that the sums of the occupancies for the cations on tetrahedral and octahedral sites are approximately 3.5 percent below that required to maintain charge balance with the framework oxygens, assuming a stoichiometric formula (Table 5). During this study we considered several explanations for this discrepancy. Unsuccessful attempts were made to account for it by adjusting the charges of the scattering factors (Wenk *et al.*, 1974), by searching for  $\text{OH}^-$  groups in the tetrahedral framework suggested by Sugiura (1959) and Iiyama (1960) which would allow vacancies on some of the tetrahedral sites, and by searching for Cl substituting for O on oxygen sites.

We now suspect that this trend is caused by the presence of cations in the channel. To maintain over-

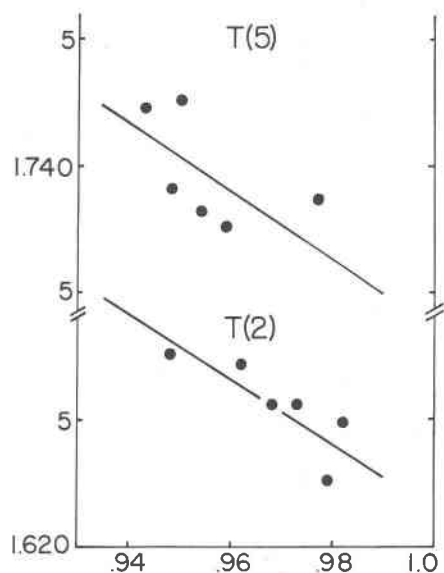


Fig. 9. Relation between mean T-O distances (ordinate) and independently refined site occupancies (abscissa) for T(2) and T(5).

all charge balance these cations must be compensated. This would be accomplished by cation vacancies in the cordierite framework. However, the actually refined occupancy of the Ch(2) site is not enough to account for the 3.5 percent cation deficiency in the framework. If it were entirely occupied by Na, as estimated from the chemical analyses, this would only account for approximately 0.3 percent vacancies of framework cations. An explanation may be that some channel cations are diffusely spread over several other channel locations, as previously suggested.

Table 5 indicates low occupancy values for both tetrahedral and octahedral sites. However, because of the possible confounding effect of Fe-Mg composition on M site occupancies, we chose not to further analyze octahedral vacancies other than to suggest their existence.

For T(1), T(3), and T(4), Figure 8 shows almost uniform occupancies when normalized to a full occupancy of 1.0 (standard deviation from the mean is approximately 0.006). T(2) and T(5) show more scatter (standard deviation from the mean is approximately 0.011) and for all samples except Sci 552 they are inversely correlated, *i.e.*, where the occupancy is low for T(2) it is high for T(5). T(2) and T(5) tetrahedra compose chains of four-member tetrahedral rings which have been emphasized by Gibbs (1966, his Fig. 7) and are therefore closely associated. If one of the two sites has a greater number of vacancies than the average for all the tetrahedral sites, the other should have fewer in order to maintain local

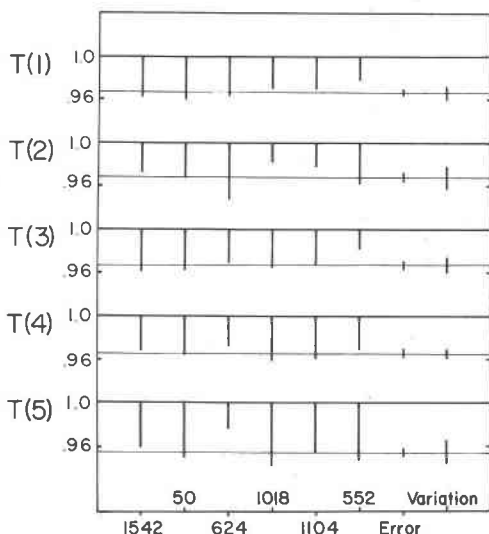


Fig. 8. Tetrahedral site occupancies, plotted as deviations from full occupancy. Variation is  $\pm$  one standard deviation from the mean for each site. Error is approximately  $\pm$  one standard deviation of each occupancy value. Note the inverse correlation of T(2) and T(5). Average occupancies for T(5) are lower than those of T(1)-T(4).

charge balance. This would explain the inverse correlation of the occupancies. Furthermore, these tetrahedra extend as *yz* layers through the structure. (100) may be a plane of preferential diffusion possibly significant in the common alteration of cordierite to the micaceous sheet silicate pinite. Because there is coupling of T(2) and T(5) occupancies, the average of vacancies on these two sites is similar to that of the other tetrahedral sites.

For both T(2) and T(5) there is a negative correlation between T–O distances and the site occupancy (Fig. 9). For T(2) and T(5) the correlation coefficient is  $r = -0.828$  and  $r = -0.546$  respectively. This indicates that a site with a greater percentage of vacancies is enlarged, which may be explained by the local excess negative charge that would exist in a vacant tetrahedron.

In Figure 6a–d there are significant positive peaks within the channel ring, particularly near O(4) and O(5) which, as we discussed earlier, have excess negative charge. We speculate that these are caused by channel cations which are stable in 6-fold or higher coordination being attracted toward tetrahedra with vacancies. These cations, possibly metal complexes, are adsorbed to those cavities on channel walls and are only coordinated on one side with oxygens of the framework.

#### *Al–Si distribution on tetrahedral sites*

A question of interest in the low-cordierite structure is the extent of substitution of Al and Si on the various tetrahedral sites. This has generally been handled by partitioning Al and Si between the sites on the basis of the mean T–O interatomic distances. T(1) is the largest site, having a mean T–O distance of 1.753Å, and is assumed to be entirely Al. The two smallest sites are T(3) and T(4), with mean T–O distances near 1.613Å. These are assumed to be entirely Si. Both of these assumptions are consistent with expected values for Si and Al (T–O) distances as determined from feldspars (Ribbe *et al.*, 1974). Relative amounts of Si and Al are then assigned to the remaining T(2) and T(5) sites having intermediate (T–O) distances on the basis of an assumed linear relationship between mean interatomic distance and Al–Si occupancy. We compare results in Table 9.

However, the above procedure may not be valid for cordierite. For one thing, there is a correlation between the directly refined occupancies of T(2) and T(5) and their mean T–O distances, two independently refined parameters (Fig. 9). In the previous section we interpreted the enlargement of these sites as the result of the substitution of vacancies for tetrahe-

Table 9. Hypothetical Al–Si substitution on T(2) and T(5) as determined from interatomic distances. Percent of total site occupancy. Derivation and limitation explained in text

Sample	Al on T(2) (%)	Si on T(5) (%)
Sci 1542	9.0	11.5
Brg 50	8.0	9.0
Sci 624	9.0	12.0
Sci 1018	7.5	8.0
Sci 1104	8.5	8.0
Sci 552	10.0	8.0

dral atoms. The variation in mean T–O distance caused in this manner accounts for most of the spread in the substitution values for each site shown in Table 9.

Actually, there may be little or no Al–Si substitution on T(2) and T(5). Cohen *et al.* (1977) studied Al–Si substitution on these sites by means of extended Hückel molecular orbital analysis (method described in Gibbs *et al.*, 1974). They showed that the slightly greater length of T(2) relative to T(3) and T(4) and the slightly smaller mean T–O distances of T(5) relative to T(1) can be explained by the relative distortions of the various tetrahedral sites. The calculations indicate that a distorted tetrahedron should have longer T–O distances (Ribbe *et al.*, 1974). This in fact is the case for T(1) and T(2) tetrahedra as Fe replaces Mg on the octahedral site, thus corroborating the molecular orbital analysis. Cohen *et al.* therefore show that Al–Si substitution is not required to explain the differences in mean T–O distances. Based on this and a direct occupancy refinement of the tetrahedral sites utilizing neutron diffraction data, they suggest that low cordierite is fully ordered as to Al and Si on tetrahedral sites. While they do not regard this as conclusive, they emphasize that small differences in mean T–O distances are not necessarily indicative of Al–Si substitution. Relying on our data, we have to concur with them and leave the question of Al–Si substitution open. However, because of the postulated presence of vacancies and their effect on interatomic distances, cordierite may not be a suitable example to study the relationship between tetrahedral distortions and Al–Si order.

#### Conclusions

In conclusion, we wish to summarize the highlights of this study and discuss their potential implications.

The first point was the distortion of the tetrahedral framework caused by Fe–Mg substitution on the octahedral site. We noticed regular linear changes, all

of which can be explained by simple adjustments of atomic positions which correlate directly with changes in lattice dimensions. As Fe substitutes for Mg, M–O distances increase while average T–O distances remain nearly constant. The structural adjustment involves the channels moving apart causing increases in *a* and *b*, a rotation and shape change of the channel rings, and the rings moving closer within each channel with a resulting decrease in *c*. Of other studied solid solutions, alkali feldspars are probably most analogous (e.g. Stewart, 1975), but here distortions are more difficult to describe. The plagioclase structure is more complicated than the cordierite structure (e.g. the split Na position in albite) and substitutions are coupled. Superstructures are created and substitutions of large cations in interstices result in changes that are not strictly linear. It is, therefore, impossible in plagioclase either to follow a continuous series or to describe distortions as being the result of a few simple principles. On the other hand, Fe–Mg substitution in olivine and chain silicates has little effect on their structure other than to expand the unit cell to allow for the enlarged octahedra. This is because of the lack of a tetrahedral framework. Cordierite is thus interesting because it stands between these examples. A continuous tetrahedral framework is present which must adjust to substitution, but both the structure and the substitution are simple enough to allow these cooperative adjustments to proceed in an orderly fashion.

Other aspects of this study concern variabilities involving the relatively large channel. We see the distribution and orientation of channel constituents, tetrahedral and octahedral site vacancies, local excess negative charge on O(4) and O(5) sites, and possible Al–Si substitution on T(2) and T(5) sites as inter-related manifestations of a fundamental variability in the cordierite structure due to local charge imbalances in the neighborhood of the channel. Channel cations must be balanced by the cation vacancies within the cordierite framework. Locations of both are influenced by the excess negative charge on O(4) and O(5), as is the orientation of channel H<sub>2</sub>O. In addition, the distribution of channel cations and the orientation of channel water seem to be interconnected. Finally, the fact that O(4) and O(5) are both present in the T(5) tetrahedron probably affects the distribution of vacancies on T(5) and, therefore, on the linked T(2) site. Likewise affected would be any Al–Si substitution on these tetrahedral sites. All these variabilities are spatially related in that they

are concentrated in the (100) plane. This suggests that they may significantly affect atomic diffusion and thereby play an important role in chemical reactions involving cordierite, including common alterations to sheet silicates. While atoms are not well positioned in the channel, they are not nearly as mobile as in zeolites. Cordierite is thus an intriguing structure with some tendencies of zeolites. Yet, in contrast to them, channel composition and framework occupancies are not independent.

It is quite surprising to find such a large number of vacancies in a silicate framework. This crystallographic "instability" may be connected with thermodynamic sensitivity to metamorphic conditions, particularly water pressure (e.g. Wood, 1973). An alternative possibility is that framework vacancies may be a more common characteristic of open silicate structures than presently supposed. Their appearance in this study would not, therefore, signify so much an "instability" of cordierite as the fact that vacancies are difficult to detect and appear only in the most precise of refinements. We are inclined to believe that vacancies of this nature are unusual, but this matter will only be resolved by vigilance for them in refinements of similar minerals.

### References

- Brown, G. E. and B. A. Mills (1980) High-temperature crystal chemistry of a hydrous alkali beryl from the Harding Pegmatite, New Mexico. *Am. Mineral.*, in press.
- Busing, W. R., K. O. Martin and H. A. Levy (1962) ORFLS A Fortran crystallographic least-squares program. *ORNL-TM-305*.
- , ——— and ——— (1964) ORFFE A Fortran crystallographic function and error program. *ORNL-TM-306*.
- Cohen, J. P., F. K. Ross and G. V. Gibbs (1977) An X-ray and neutron diffraction study of hydrous low cordierite. *Am. Mineral.*, 62, 67–78.
- Cromer, D. T. (1965) Anomalous dispersion corrections computed from self-consistent field relativistic Dirac-Slater wave functions. *Acta Crystallogr.*, A18, 17–23.
- and J. B. Mann (1968) X-ray scattering factors computed from numerical Hartree-Fock wave functions. *Acta Crystallogr.*, A24, 321–324.
- Farrell, E. F. and R. E. Newnham (1967) Electronic and vibrational absorption spectra in cordierite. *Am. Mineral.*, 52, 380–388.
- Gibbs, G. V. (1966) The polymorphism of cordierite: I. The crystal structure of low cordierite. *Am. Mineral.*, 51, 1068–1087.
- , S. J. Louisnathan, P. H. Ribbe and M. W. Phillips (1974) Semi-empirical molecular orbital calculations for atoms of the tetrahedral framework in anorthite, low albite, maximum microcline and reedmergerite. In W. S. MacKenzie and J. Zussman, Eds., *The Feldspars*, p. 49–67. Manchester University Press, Manchester.
- Goldman, D. S., G. R. Rossman and W. A. Dollase (1977) Channel constituents in cordierite. *Am. Mineral.*, 62, 1144–1157.

- Hochella, M. F., Jr., G. E. Brown, Jr., F. K. Ross and G. V. Gibbs (1979) High-temperature crystal chemistry of hydrous Mg- and Fe-rich cordierites. *Am. Mineral.*, 64, 337-351.
- Iiyama, T. (1960) Recherches sur le rôle de l'eau dans la structure et la polymorphisme de la cordierite. *Bull. Soc. fr. Minéral. Cristallogr.*, 83, 155-178.
- Meagher, E. P. (1967) *The Crystal Structure and Polymorphism of Cordierite*. Ph.D. Thesis, The Pennsylvania State University, University Park, Pennsylvania.
- Miyashiro, A. (1957) Cordierite-indialite relations. *Am. J. Sci.*, 255, 43-62.
- Ribbe, P. H., M. W. Phillips and G. V. Gibbs (1974) Tetrahedral bond length variations in feldspars. In W. S. MacKenzie and J. Zussman, Eds., *The Feldspars*, p. 25-48. Manchester University Press, Manchester.
- Schreyer, W. (1966) Synthetische und natürliche Cordierite III. Polymorphiebeziehungen. *Neues Jahrb. Mineral. Abh.*, 105, 211-244.
- and H. S. Yoder (1964) The system Mg-cordierite-H<sub>2</sub>O and related rocks. *Neues Jahrb. Mineral. Abh.*, 101, 271-342.
- Smith, J. V. and W. Schreyer (1960) Location of argon and water in cordierite. *Mineral. Mag.*, 33, 226-236.
- Stewart, D. B. (1975) Lattice parameters, composition and Al/Si order in alkali feldspars. In P. H. Ribbe, Ed., *Feldspar Mineralogy*, Chapter 3. Short Course Notes Vol. 2, Mineralogical Society of America, Washington, D. C.
- Sugiura, K. (1959) The water problem of cordierite. *Bull. Tokyo Inst. Tech., Ser. B, I*, 1-26.
- Tsang, T. and S. Ghose (1972) Nuclear magnetic resonance of <sup>1</sup>H and <sup>27</sup>Al and Al-Si order in low cordierite, Mg<sub>2</sub>Al<sub>4</sub>Si<sub>5</sub>O<sub>18</sub> · nH<sub>2</sub>O. *J. Chem. Phys.*, 56, 3329-3332.
- Wenk, H. R. and K. N. Raymond (1973) Four new structure refinements of olivine. *Z. Kristallogr.*, 137, 86-105.
- , E. Wenk and J. H. Wallace (1974) Metamorphic mineral assemblages in pelitic rocks of the Bergell Alps. *Schweiz. Mineral. Petrogr. Mitt.*, 54, 508-554.
- Wood, B. J. (1973) Fe<sup>2+</sup>-Mg<sup>2+</sup> partition between coexisting cordierite and garnet—a discussion of the experimental data. *Contrib. Mineral. Petrol.*, 40, 253-258.
- Zachariasen, W. H. (1968) Experimental tests of the general formula for the integrated intensity of a real crystal. *Acta Crystallogr.*, A24, 212-216.

Manuscript received, October 10, 1978;  
accepted for publication, July 23, 1979.